Nonlinear instability and chaos in plasma wave–wave interactions. II. Numerical methods and results

C. S. Kueny and P. J. Morrison
Department of Physics and Institute for Fusion Studies, The University of Texas at Austin, Austin, Texas 78712

(Received 17 April 1995; accepted 3 August 1995)

In Part I of this work [Phys. Plasmas **2**, 1926 (1995)], the behavior of linearly stable, integrable systems of waves in a simple plasma model was described using a Hamiltonian formulation. Explosive instability arose from nonlinear coupling between positive and negative energy modes, with well-defined threshold amplitudes depending on the physical parameters. In this concluding paper, the nonintegrable case is treated numerically. The time evolution is modeled with an explicit symplectic integrator derived using Lie algebraic methods. For amplitudes large enough to support two-wave decay interactions, strongly chaotic motion destroys the separatrix bounding the stable region in phase space. Diffusive growth then leads to explosive instability, effectively reducing the threshold amplitude. For initial amplitudes too small to drive decay instability, slow growth via Arnold diffusion might still lead to instability; however, this was not observed in numerical experiments. The diffusion rate is probably underestimated in this simple model. © *1995 American Institute of Physics.*

I. INTRODUCTION

In this paper we continue the treatment of chaos in plasma wave–wave interactions begun in a companion paper,[1] which we refer to as Part I. In Part I the simple beam plasma model to be studied was introduced, the Hamiltonian structure of the model was elucidated, and normal mode variables representing ion-acoustic modes were derived. The behavior of sets of two or three modes interacting via a single nonlinear coupling term was described.

Here we discuss the behavior of larger numbers of modes interacting via two or three nonlinear terms in the Hamiltonian (and thus comprising two and three degree-of-freedom systems). Such systems are nonintegrable, necessitating the use of numerical methods. It is demonstrated that the intrinsically chaotic behavior of such systems has a profound effect on their stability. The problems treated in Part I and here are of general importance in Hamiltonian dynamics with a long history of application in fluid and plasma physics. (See, e.g., the references of Part I; also Ref. 2 and references therein).

In Sec. II we describe the numerical method used. After a brief discussion of symplectic integration algorithms in general, we focus on the use of Lie transforms to obtain explicit expressions for time advancing the dynamical variables.[3–7] In Sec. III we present numerical results for a number of systems described by Hamiltonians of one, two, and three degrees of freedom. We demonstrate the role of chaotic diffusion in destabilizing such systems. Section IV provides a summary and conclusions.

II. SYMPLECTIC INTEGRATION USING LIE TRANSFORMS

As discussed in Part I, chaotic motion in a system of waves allows phase space diffusion that can have dramatic consequences for long-term stability. At the same time, the Hamiltonian nature of the phase space may place strict limits on the possible motion. In doing numerical work, therefore, we must ensure that the Hamiltonian structure is properly reproduced, so that the observed chaotic motion and phase space diffusion are true properties of the Hamiltonian and not spurious results of the numerical method. This is facilitated by symplectic integration methods. (For a review of such methods, see Ref. 8 and the references therein.)

A major drawback of many symplectic algorithms is that they are implicit. For example, the well-known Runge–Kutta algorithm is symplectic when expressed in implicit form.[9,10] The solution of the implicit equations turns out to be very problematic for some of the systems of interest here. An alternative approach that provides an explicit symplectic algorithm involves the application of Lie transforms.[4] We show presently how this method is used to obtain an explicit, small time step integrator. Besides eliminating troublesome implicit formulas, this algorithm was three times faster than Runge–Kutta for systems of interest in this paper.

In Ref. 4, Dragt and Forest show that for any polynomial Hamiltonian, the time evolution of the dynamical variables z_i may be expressed as a product of operators,

$$z_i' = \mathscr{M} z_i := \cdots e^{[f_4,\cdot]} e^{[f_3,\cdot]} e^{[f_2,\cdot]} z_i , \tag{1}$$

where f_n is a homogeneous polynomial of degree n. Each operator $e^{[f_n,\cdot]}$ is evaluated by expanding the exponential:

$$e^{[f_n,\cdot]} z_i := z_i + [f_n, z_i] + \frac{1}{2!}[f_n,[f_n,z_i]] + \frac{1}{3!}[f_n,[f_n,[f_n,z_i]]] + \cdots , \tag{2}$$

where $[f,g]$ is the usual Poisson bracket,

$$[f,g] = \sum_{i=1}^{N} \left(\frac{\partial f}{\partial q_i}\frac{\partial g}{\partial p_i} - \frac{\partial g}{\partial q_i}\frac{\partial f}{\partial p_i} \right), \tag{3}$$

that acts on any functions f and g of the dynamical variables. A transformation of the form (2) is an example of a Lie transform.

Each operator in the product (1) describes a symplectic transformation, and the product of any number of such operators is likewise symplectic. Each nth-order operator $e^{[f_n,\cdot]}$ in the product represents the action of the nth-order terms in the Hamiltonian H. If this infinite product is truncated at any order n, then the remaining finite product of operators will describe the motion accurately up to order $n-1$ in the dynamical variables.

The functions f_2 and f_3 (all that we will require) in (1) are found as follows. If the Hamiltonian is $H=H_2+H_3+\cdots$, where H_n denotes terms of order n, then the polynomial f_2 is given simply by

$$f_2=-H_2\Delta t. \tag{4}$$

The polynomial f_3 is given by the integral of H_3 over the lowest-order orbits,

$$f_3:=\int_0^{\Delta t} dt\ H_3(z_i'), \tag{5}$$

where $H_3(z_i')$ means the polynomial H_3 evaluated at $z_i'=e^{[f_2,\cdot]}z_i$.

Any operator $e^{[f_n,\cdot]}$ for $n>2$ will, in general, yield an infinite series containing all powers of the z_i; the series cannot be truncated at any order without destroying the symplectic property.[6] It turns out, however, that closed-form expressions exist for the general operator.[7] As a first step in obtaining such expressions, it is often desirable to decompose the polynomial operator into a product of monomial and/or polynomial operators via the Campbell–Baker–Hausdorff theorem.[3] It is easily found that a cubic polynomial operator $e^{[f_3,\cdot]}$ may be approximately reexpressed as a product of operators:

$$e^{[f_3,\cdot]}:=\exp\left(\left[\sum_{i=1}^{N} f_3^{(i)},\cdot\right]\right)\approx\prod_{i=1}^{N}\left(e^{[f_3^{(i)},\cdot]}\right), \tag{6}$$

where the error is of fourth order in the $\hat{z}_i$.

After decomposing an operator into such constituent operators, the resulting operators are then used to obtain explicit transformations. For a function f_1 that is linear in the dynamical variables (p_i,q_i), the resulting transformation truncates at first order. For a quadratic function f_2, the resulting transformation is linear; the infinite series is summed to give the constant coefficients. For a monomial f_n of cubic or higher order, general closed form expressions have been derived by Gjaja.[7] Specific examples will be described in the Appendix.

An alternative method of obtaining explicit polynomial transformations from Lie operators was developed in Ref. 5. This method, known as kick-factorization, consists of finding, for any polynomial operator $e^{[f_n,\cdot]}$, a new operator $e^{[g_n,\cdot]}$, where g_n has terms of the form $\alpha(ap+bq)^n$. The series expansion for such an operator terminates at order $n-1$, so that the full transformation for the time advance may be written as a composition of explicit polynomial transformations. This method was used in an earlier version of the work described here,[11] but its application is more difficult than the method of Ref. 7, which was used to produce the results in this paper.

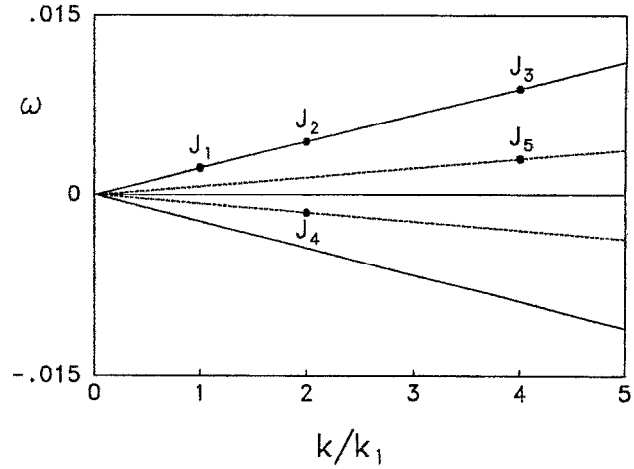

FIG. 1. Five modes comprising a negative-energy resonance and two positive-energy near resonances.

III. NUMERICAL RESULTS

We now present numerical results for several simple systems of interest. Results are grouped according to the number of degrees of freedom, which will correspond to the number of nonlinear terms included in the Hamiltonian. Three cases are considered: one degree of freedom (to see how well our algorithm reproduces the known integrable motion); two degrees of freedom (to examine the effect of nonintegrability and resultant separatrix breaking in the simplest case); and three degrees of freedom (to study the effect of strong chaos on explosive instabilities).

The systems to be considered will comprise various subsets of the set of ion-acoustic modes shown in Fig. 1. As described in Part I, the "negative-energy resonance" between modes J_2, J_4 and J_5 leads to explosive instability, while the near-resonant interaction among the modes J_1, J_2, and J_3 leads to decay instabilities. The only positive-energy resonances considered in this paper will be these near resonances that occur generically for pairs of long-wavelength modes. Three-wave positive energy resonances may also be important in generating chaotic motion, although only in isolated regions of parameter space. The effect of such resonances on explosive instabilities, discussed in Ref. 11, is omitted here.

The normalization introduced in Part I was such that time is measured in units of the inverse ion plasma frequency ω_p^{-1}. The actual characteristic frequency of an ion-acoustic oscillation with wave number $k_1:=2\pi/L$ is k_1c_s in physical variables, or k_1 in our dimensionless variables. For computations we therefore renormalize by multiplying the Hamiltonian and time by $1/k_1$ and k_1, respectively, so that one unit of time now corresponds to one ion-acoustic oscillation time k^{-1}. To make the Hamiltonian's coefficients closer to unity, it is multiplied again by a factor of 10^4, so that the unit of

time finally used in computations is ten thousand ion-acoustic oscillation times, $10^4/k_1$.

A. Integrable cases

Before looking at numerical studies of chaos, we first check that our algorithm properly reproduces the known behavior of the integrable, single-resonance systems. We consider both a two-wave positive energy resonance and a three-wave negative energy resonance.

1. Positive energy resonance

The numerical method is first applied to the single two-wave doublet described by the Hamiltonian of Eq. (71) of Part I:

$$H=\omega_1 J_1+\omega_2 J_2+\alpha J_1\sqrt{J_2}\,\sin(2\theta_1-\theta_2). \tag{7}$$

Modes J_1 and J_2 (seen in Fig. 1) have wave numbers k_1 and $2k_1$, respectively, where $k:=2\pi/L$. (Thus J_1 is the longest-wavelength mode possible in our system of size L.) In terms of the "resonance variables,"

$$\begin{aligned} &I_1=\tfrac{1}{2}J_1, \quad \psi_1=2\theta_1-\theta_2,\\ &I_3=\tfrac{1}{2}J_1+J_2, \quad \psi_3=\theta_2, \end{aligned} \tag{8}$$

this takes the form

$$\begin{aligned} \bar{H}&=\Omega_1 I_1+2\alpha I_1\sqrt{I_3-I_1}\,\sin\psi_1\\ &=\frac{\Omega_1}{2}\,(P_1^2+Q_1^2)\\ &\quad+\alpha Q_1\sqrt{(P_1^2+Q_1^2)(I_3-\tfrac{1}{2}\,(P_1^2+Q_1^2))}, \end{aligned} \tag{9}$$

where

$$P_1=\sqrt{2I_1}\,\cos\psi_1, \qquad Q_1=\sqrt{2I_1}\,\sin\psi_1, \quad I_3=\text{const},$$

and

$$\Omega_1=2\omega_1-\omega_2.$$

While the resonance variables are convenient ones in which to view the phase space topology, numerical computations were carried out using coordinates $(\hat{P}_i,\hat{Q}_i)$ introduced in the Appendix, where the Lie algorithm used is also described. For the discussion here we need refer only to the resonance variables; the transformations between these and the $(\hat{P}_i,\hat{Q}_i)$ were done internally by the computer.

In Fig. 2 we plot Q_1 vs. P_1 for the Hamiltonian of Eq. (9); the parameters ($\Lambda=100$, $L=5000$, $v=1.4796$) here are the same as in Fig. 3(b) of Part I; the time step used was $\Delta t=0.2$. (Recall Λ, L, and v measure one-dimensional plasma parameter, box size, and drift velocity, respectively.) Good agreement with the analytical curves is observed. Our numerical algorithm was iterated up to time corresponding to 3.5×10^6 ion-acoustic periods (or $t=350$ in computational time units) for each of the orbits shown; this provided enough data points to illustrate the curves clearly. In order to assess the long-time effects of numerical error, single curves from Fig. 2 have also been calculated for $0<t<10^{10}$ ion-acoustic periods (5×10^6 computational time steps). As with most of the work to be described in this paper, computations

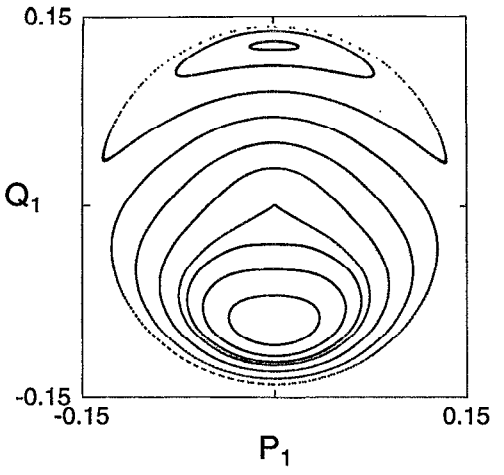

FIG. 2. Numerical orbits for the Hamiltonian (7), with $\Lambda=100$, $L=5000$, and $v=1.4796$.

were done using 64-bit arithmetic (i.e., 15–16 digit precision). No numerical diffusion of the orbit was observed.

2. Negative energy resonance

We now consider the three-wave negative energy resonance described by the Hamiltonian of Eq. (87) of Part I:

$$H=\omega_2 J_2-\omega_4 J_4-\omega_5 J_5+\gamma\sqrt{J_2 J_4 J_5}\,\sin(\theta_2+\theta_4+\theta_5). \tag{10}$$

The modes J_2, J_4, and J_5 are illustrated in Fig. 1. In terms of the resonance coordinates,

$$\begin{aligned} &I_3=J_2, \quad \psi_3=\theta_2+\theta_4+\theta_5,\\ &I_4=J_4-J_2, \quad \psi_4=\theta_4,\\ &I_5=J_5-J_2, \quad \psi_5=\theta_5, \end{aligned} \tag{11}$$

introduced in Part I, this Hamiltonian takes the form

$$\bar{H}=\Omega_3 I_3+\gamma\sqrt{I_3(I_4+I_3)(I_5+I_3)}\,\sin\psi_3, \tag{12}$$

where $\Omega_3=\omega_2-\omega_4-\omega_5$, $I_4=\text{const}$, and $I_5=\text{const}$. For the special case $I_4=I_5=0$ (corresponding to $J_2=J_4=J_5$), the Hamiltonian reduces to the polynomial form

$$\begin{aligned} \bar{H}&=\Omega_3 I_3+\gamma I_3^{3/2}\,\sin\psi_3\\ &=\frac{\Omega_3}{2}\,(P_3^2+Q_3^2)+\frac{\gamma}{2\sqrt{2}}\,Q_3(P_3^2+Q_3^2), \end{aligned} \tag{13}$$

where $P_3=\sqrt{2I_3}\,\cos\psi_3$ and $Q_3=\sqrt{2I_3}\,\sin\psi_3$. In this form the Hamiltonian is now amenable to the Lie transform methods described in Sec. II.

In Fig. 3 we reproduce Fig. 6(b) of Part I, showing the phase space for the Hamiltonian of (13) for the parameters $\Lambda=100$, $L=5000$, and $v=1.479\,592\,56$ ($\Omega_3\neq0$). The translation from the dimensionless variables (P_3,Q_3) back to physical variables is given by

$$|E|=\mathscr{B}\sqrt{P_3^2+Q_3^2}, \tag{14}$$

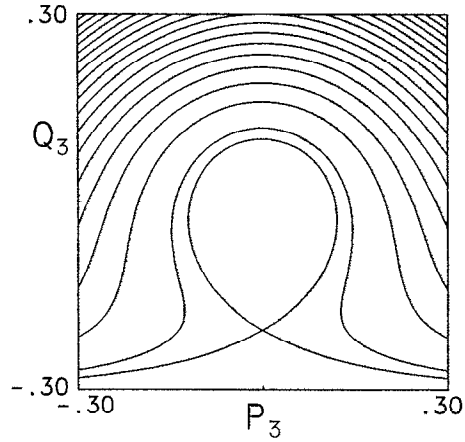

FIG. 3. Phase space plots for Hamiltonian (13) with $I_4=I_5=0$, $\Lambda=100$, $L=5000$, and $v=1.479\,592\,6$ ($\Omega_3\neq 0$).

where E is the electric field magnitude for the mode $J_2\equiv I_3\equiv(P_3^2+Q_3^2)/2$ in units of $T_e/e\lambda_d$, the constant $\mathscr{A}$ is

$$\mathscr{A}:=\left(2\Lambda L\,\frac{\partial\epsilon(k,\omega)}{\partial\omega}\right)^{-1/2}, \tag{15}$$

and ϵ is the dielectric function,

$$\epsilon(k,\omega):=1+\frac{1}{k^2}-\frac{1}{2}\left(\frac{1}{(\omega-kv)^2}+\frac{1}{(\omega+kv)^2}\right). \tag{16}$$

For the parameters of Fig. 3, $\mathscr{A}\approx 7.7\times10^{-8}$. Thus, for a Debye length $\lambda=0.005$ cm and an electron temperature of 0.65 keV, the distance from the origin gives the electric field of this mode in V/m.

Curves obtained by numerically iterating the Lie transform for the Hamiltonian of this system are shown in Fig. 4; good agreement with the analytical curves of Fig. 3 is seen. The orbits shown were computed for total times ranging from 10^6–10^8 ion-acoustic periods. Some orbits were again iterated up to $t=10^{10}$ ion-acoustic periods to check for any numerical diffusion; none was observed.

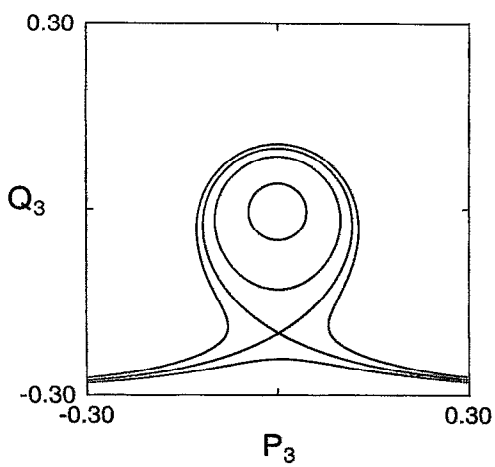

FIG. 4. Numerical orbits for the Hamiltonian (13) with the same parameters seen in Fig. 3.

B. Nonintegrability: Two degrees of freedom

We now consider a nonintegrable Hamiltonian with two degrees of freedom. The case examined here involves the interaction of two positive-energy resonances. The interaction of a single positive-energy resonance with a single negative-energy resonance, less relevant to our purposes here, was discussed in Ref. 11.

Consider the Hamiltonian describing the interaction of the three positive energy modes shown in Fig. 1:

$$H=\omega_1J_1+\omega_2J_2+\omega_3J_3+\alpha J_1\sqrt{J_2}\,\sin(2\theta_1-\theta_2)+\beta J_2\sqrt{J_3}\,\sin(2\theta_2-\theta_3). \tag{17}$$

The transformation to resonance variables is

$$\begin{aligned} &J_1=2I_1, \quad \psi_1=2\theta_1-\theta_2,\\ &J_2=I_3-2I_2-I_1, \quad \psi_2=\theta_3-2\theta_2,\\ &J_3=I_2, \quad \psi_3=\theta_2, \end{aligned} \tag{18}$$

which yields

$$\bar{H}=H-\omega_2I_3=\Omega_1I_1+\Omega_2I_2+\alpha 2I_1\sqrt{I_3-2I_2-I_1}\,\sin\psi_1-\beta(I_3-2I_2-I_1)\sqrt{I_2}\,\sin\psi_2, \tag{19}$$

where $\Omega_2=\omega_3-2\omega_2$ and $I_3=\frac{1}{2}J_1+J_2+2J_3=$const. If the mode I_1 was absent from this Hamiltonian, we would have the Hamiltonian (84) of Part I, with the phase space structure shown in Fig. 4 of that paper. If instead the mode I_2 was absent, we would have the Hamiltonian (75) of Part I [Eq. (9) of this paper], with the phase space structure seen in Fig. 3 of that paper and partially reproduced in Fig. 2 of this paper. We saw that that Hamiltonian had an unstable fixed point at the origin when $|\Omega_1/\alpha|<2\sqrt{I_3}$; we expect a condition close to that to also hold for the Hamiltonian (19). It is along the separatrix associated with this unstable fixed point that chaotic motion will arise.

Surface of section plots for the Hamiltonian (19) are shown in Fig. 5 for $\Lambda=100$, $v=1.4796$, and L ranging from 2500 to 15 000. The constant I_3 was set to 0.01; the time step was again $\Delta t=0.2$. The orbits of Figs. 5(a) and 5(b) were computed to times of $t=2\times10^8$ and $t=10^9$ ion-acoustic periods, respectively. For each orbit, initial conditions are $P_2=0$, $Q_2=10^{-6}$ ($\psi_2=\pi/2$, $I_2=5\times10^{-13}$). The variables (P_1,Q_1) are initialized at a sampling of values, and are plotted each time that ψ_2 passes through $\pi/2$. (Since the time step must remain constant to preserve symplecticity, the actual points plotted are determined by linear interpolation between the values immediately before and after the orbit passes through the $\psi_2=\pi/2$ plane.) Note that the various orbits in each plot correspond to different values of $\bar{H}$; these values are nearly equal to the values for the orbits plotted in Fig. 2, for which the mode I_2 was absent. Now, however, the second nonlinear term in (19) will lead to growth of I_2 via decay instability, with a strong perturbing effect on the system.

The phase space topology is determined primarily by the effective detunings Ω_1/α and Ω_2/β, which are both proportional to $k_1\equiv 1/L$. The smaller the magnitudes of these two quantities, the more chaotic the system's behavior will be. For $L=2500$ ($\Omega_1/\alpha\approx 0.19$, $\Omega_2/\beta\approx -0.53$) a very thin chaotic

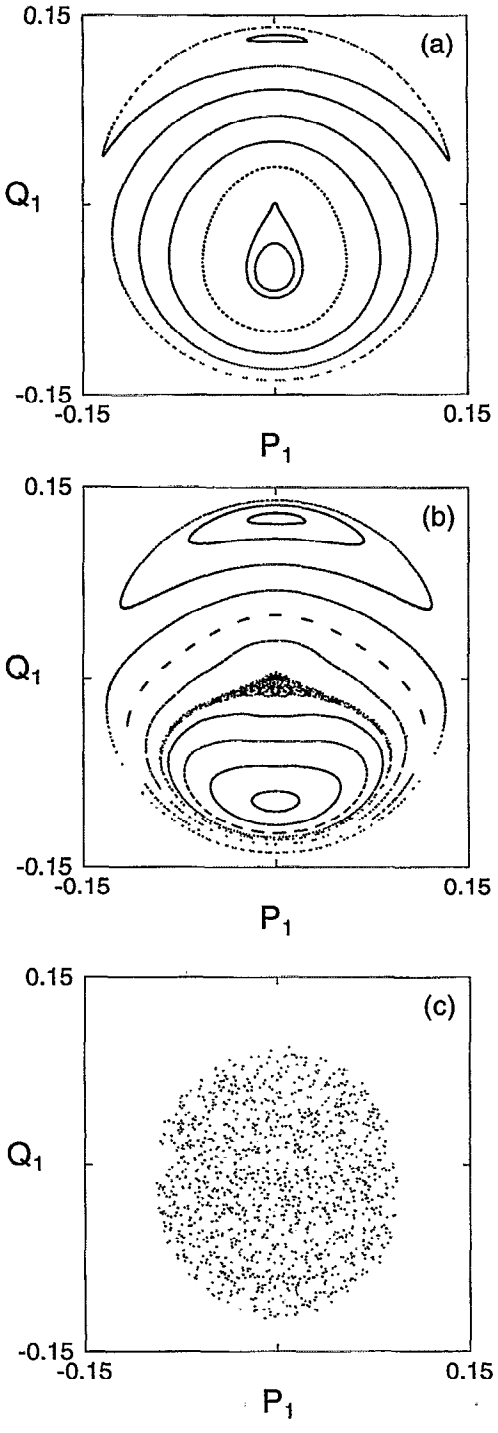

FIG. 5. The $P_2=0$ surface of section plots for Hamiltonian (19), with (a) $L=2500$; (b) $L=5000$; and (c) $L=15\,000$. Each orbit was started with $Q_2=10^{-6}$, so that each corresponds to a different value of $\bar{H}$.

layer exists along the separatrix through the fixed point at the origin. For $L=5000$ ($\Omega_1/\alpha\approx 0.09$, $\Omega_2/\beta\approx -0.27$), the chaotic layer through the origin has become more prominent, and when $L=15\,000$ ($\Omega_1/\alpha\approx 0.04$, $\Omega_2/\beta\approx -0.09$) most of the accessible phase space is occupied by chaotic orbits; all points shown in Fig. 5(c) are part of a single such orbit.

C. Chaotic transport in three degrees of freedom

We now consider a system consisting of all five of the modes seen in Fig. 1. Modes J_2, J_4, and J_5 form a negative-energy triplet, while mode J_2 forms two near resonances with modes J_1 and J_3. We have seen that the two near resonances involving modes J_1, J_2, and J_3 can generate strongly chaotic motion, depending on the value of k_1. The negative-energy resonance will drive explosive instability when $\Omega_3=0$ is satisfied, so that almost any perturbation will lead to immediate explosive growth. By changing v we detune this resonance, opening an islet of stable motion around $I_3=0$. If the system is strongly chaotic then fast diffusion can occur in phase space, allowing initially "stable" orbits to attain large enough amplitude for explosive instability to occur. If the motion is mostly regular, this fast diffusion will not occur. The many three-dimensional invariant surfaces existing in that case cannot partition the five-dimensional energy surface, however, so that even an orbit lying in the thinnest chaotic layer near the origin may in principle still find its way to large amplitude and subsequent explosive growth.[12,13] This process (Arnold diffusion) is generally quite slow.

This system is of course much simpler than is likely to occur in reality. In general, many more modes would be present and interacting via two-wave near resonances, which would likely provide faster diffusion rates. However, the system is of interest as the simplest highly chaotic system of more than two degrees of freedom that we can obtain from our counterstreaming ion model.

The Hamiltonian for the five-wave set is given by

$$\begin{aligned} H=&\omega_1 J_1+\omega_2 J_2+\omega_3 J_3-\omega_4 J_4-\omega_5 J_5 \\ &+\alpha J_1\sqrt{J_2}\,\sin(2\theta_1-\theta_2)+\beta J_2\sqrt{J_3}\,\sin(2\theta_2-\theta_3) \\ &+\gamma\sqrt{J_2 J_4 J_5}\,\sin(\theta_2+\theta_4+\theta_5). \end{aligned} \tag{20}$$

The transformation to resonance variables is given by

$$\begin{aligned} &J_1=2I_1, \quad \psi_1=2\theta_1-\theta_2, \\ &J_2=I_3-2I_2-I_1, \quad \psi_2=\theta_3-2\theta_2, \\ &J_3=I_2, \quad \psi_3=\theta_2+\theta_4+\theta_5, \\ &J_4=I_4+I_3, \quad \psi_4=\theta_4, \\ &J_5=I_5+I_3, \quad \psi_5=\theta_5, \end{aligned} \tag{21}$$

which yields the three degree-of-freedom Hamiltonian,

$$\begin{aligned} \bar{H}=&H+\omega_4 I_4+\omega_5 I_5 \\ =&\Omega_1 I_1+\Omega_2 I_2+\Omega_3 I_3+\alpha 2I_1\sqrt{I_3-2I_2-I_1} \\ &\times\sin\psi_1-\beta(I_3-2I_2-I_1)\sqrt{I_2}\,\sin\psi_2 \\ &+\gamma\sqrt{(I_3-2I_2-I_1)(I_4+I_3)(I_5+I_3)}\,\sin\psi_3, \end{aligned} \tag{22}$$

where $I_4=J_4-(\frac{1}{2}J_1+J_2+2J_3)=\text{const}$ and $I_5=J_5-(\frac{1}{2}J_1+J_2+2J_3)=\text{const}$. We will consider the case $I_4=I_5=0$, for which the Hamiltonian can be transformed to a three degree-of-freedom polynomial, as described in the Appendix.

We consider initial states where modes J_2, J_4, and J_5 (those involved in the explosive instability) are of significant (and approximately equal) amplitude, while modes J_1 and J_3 begin with very small amplitudes. In the transformed vari-

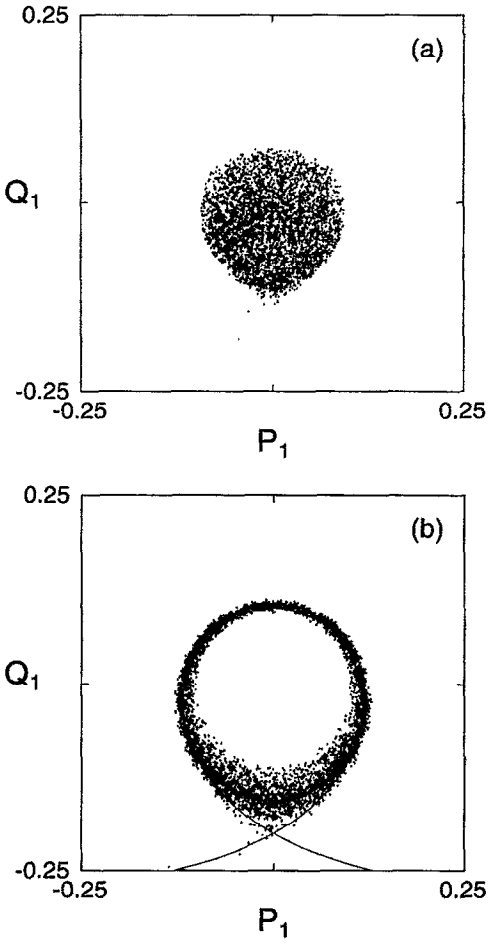

FIG. 6. Surface of section plots of (a) Q_1 vs P_1 and (b) Q_3 vs P_3, for $L=5000$ and $Q_3(0)=-0.1513$. Escape occurred at $t\approx 2.8\times 10^9$ ion-acoustic periods.

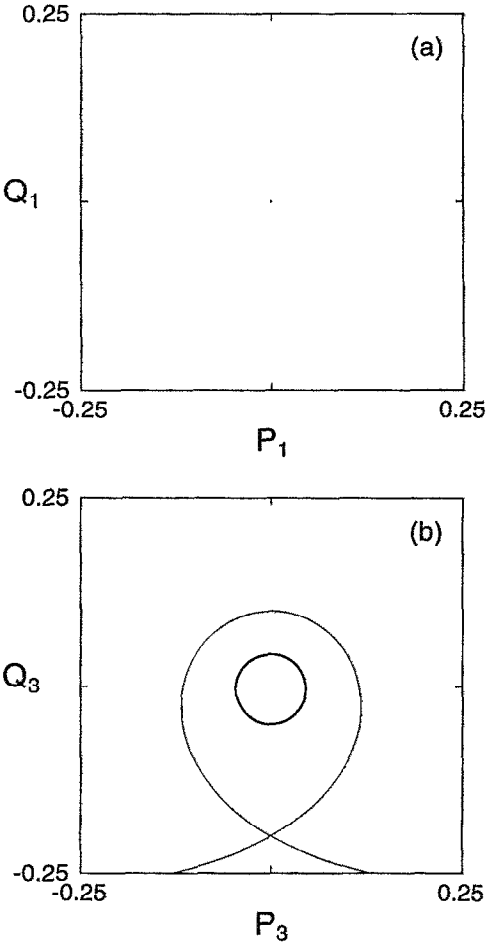

FIG. 7. Surface of section plots of (a) Q_1 vs P_1 and (b) Q_3 vs P_3, for $L=5000$ and $Q_3(0)=-0.05$. No growth in amplitude of I_3 is visible at $t=10^{10}$ ion-acoustic periods.

ables, this means that I_3 starts with a significant amplitude, while I_1 and I_2 are small. We will therefore see what is essentially a perturbation of the constant energy curves of Fig. 3 due to the coupling to modes I_1 and I_2. We again expect that if the mode I_3 has amplitude above a threshold given roughly by $\sqrt{I_3} > |\Omega_1/2\alpha|$, then we will have the possibility of chaotic motion arising from decay instabilities. This chaotic motion will then drive diffusion in the value of I_3. If the initial value of I_3 is below this threshold, we expect the motion to be mostly regular and any diffusion to be slow.

Fixing the value $\Lambda=100$, we examined various system sizes L. For each value of L, the equilibrium drift speed v was chosen so that the "unperturbed" separatrix would be of the size seen in Fig. 3. The system was always initialized with the values $(P_1,Q_1)=(P_2,Q_2)=(0,10^{-6})$. The time step was $\Delta t=0.2$. An arbitrary amplitude of 100 was chosen to indicate "escape" if any of the computational variables $(\hat{P}_i,\hat{Q}_i)$ became larger than this. The growth of amplitudes from $(\hat{P}_i,\hat{Q}_i)<1$ to $(\hat{P}_i,\hat{Q}_i)\gg 100$ occurs very quickly once explosive growth sets in. Mode amplitudes are not monitored once this occurs; we are interested only in how the modes achieve sufficient amplitude for this growth to begin.

Surface of section plots ($\psi_2=\pi/2$) for $L=5000$ are shown in Figs. 6 and 7, and for $L=15\,000$ in Figs. 8 and 9. All initial values of (P_3,Q_3) were chosen well within the unperturbed separatrix, which is indicated by a solid line. For reference, the separatrix passes through the points (0, 0.1) and (0, −0.2). For $L=5000$, the orbit shown in Fig. 6 has an initial value of $I_3=(P_3^2+Q_3^2)/2$ sufficiently large that the evolution of both I_1 and I_3 is strongly chaotic, and I_3 eventually experiences explosive growth. (Interestingly, the orbit spends some time near amplitudes associated with the separatrix before explosive growth occurs.) For another orbit initialized with much smaller I_3 (Fig. 7), there is no growth of I_1 from its initial small value, and the motion is very regular. No diffusion in I_3 was observed during 10^{10} ion-acoustic periods.

For $L=15\,000$, explosive growth sets in at a much smaller wave amplitude (Fig. 8). With an even smaller initial amplitude of I_3, we see a very restricted chaotic layer in the (P_1,Q_1) motion, and no visible diffusion in I_3 was observed by the end of 10^{10} ion-acoustic periods (Fig. 9).

For the orbit of Fig. 8, the electric field magnitude E for mode $I_3=J_2$ is plotted as a function of time in Fig. 10. (The data in this figure comprise the electric field only at times for which points were plotted in Fig. 8; these discrete points are

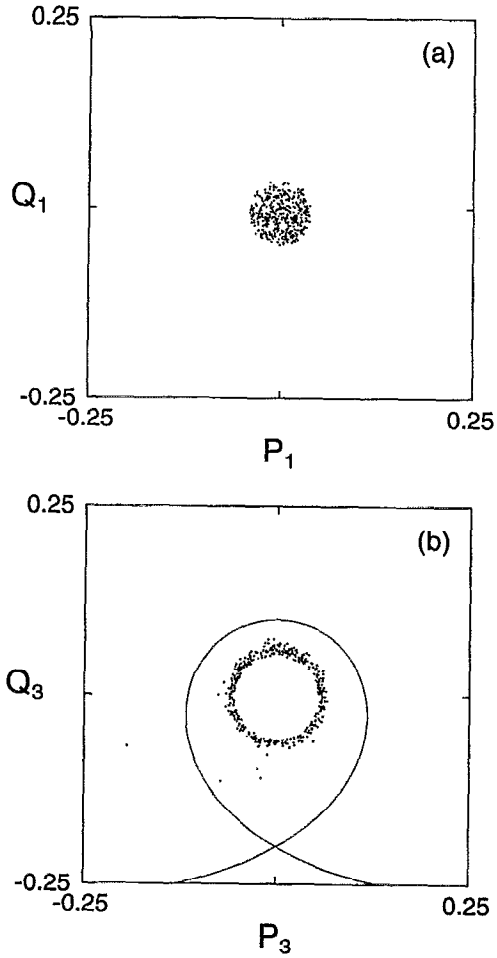

FIG. 8. Surface of section plots of (a) Q_1 vs P_1 and (b) Q_3 vs P_3, for $L=15\,000$ and $Q_3(0)=-0.06$. Escape occurred at $t\approx 8.4\times 10^8$ ion-acoustic periods.

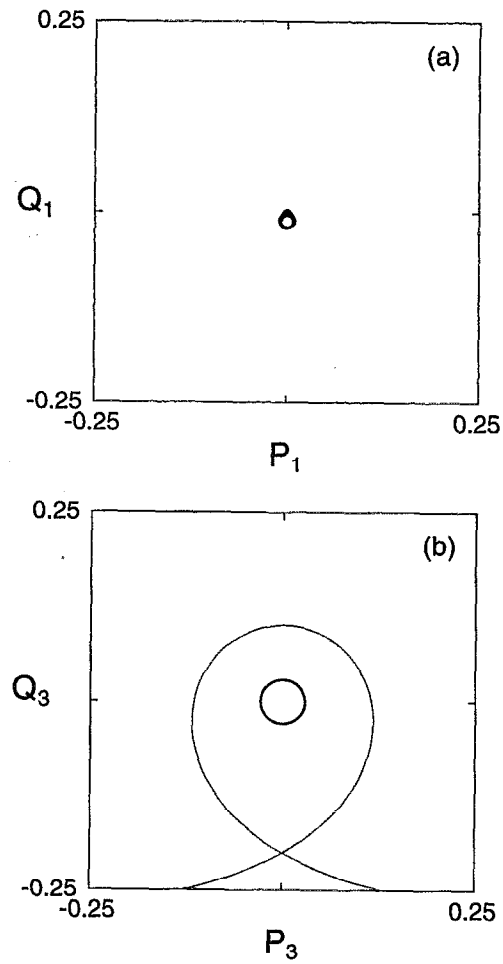

FIG. 9. Surface of section plots of (a) Q_1 vs P_1, and (b) Q_3 vs P_3, for $L=15\,000$ and $Q_3(0)=-0.03$. No growth in amplitude of I_3 is visible at $t=10^{10}$ ion-acoustic periods.

connected with straight lines.) The steady growth in amplitude over time is evident, until explosive growth takes over.

For the case $L=5000$, Fig. 11 shows the escape time as a function of initial value $Q_3(0)$, for $P_3(0)=0$. Initial values of Q_3 were chosen progressively closer to the origin, until for one of them the arbitrarily chosen time $t=2\times 10^{10}$ ion-acoustic periods was reached without escape; the value of $|Q_3(0)|$ for which this occurs will be denoted $|Q_3|_{\max}$, for the "maximum" stable value. The sharp rise of escape time near $|Q_3|_{\max}$ occurred for all values of L, but the precise value of $|Q_3|_{\max}$ was strongly dependent on L. These regions of sharply rising escape times may be thought of as defining an effective boundary for stability, i.e., a "reduced separatrix."

Figure 12(a) shows $|Q_3|_{\max}$ as a function of L; Fig. 12(b) shows the same data where Q_3 has been translated back to the electric field E. For the integrable system of Eq. (13), the largest stable perturbation would be at $|Q_3(0)|=0.2$; this is indicated by the dotted line in Fig. 12(b). We see that the reduced separatrix size decreases with increasing wavelength, due to the strong chaos generated by two-wave interactions.

Since a defining characteristic of chaotic motion is extreme sensitivity to initial conditions, orbits that start very near one another will in general evolve quite differently. Plots such as those of Figs. 11 and 12, each point of which represents a single orbit, will therefore be extremely spiky. Another consequence of the sensitive dependence on initial conditions is that it is intrinsically impossible to accurately follow a chaotic orbit with any finite-precision algorithm, since roundoff error will grow exponentially. "Shadowing" arguments may be invoked to show that in cases where the numerical algorithm is not following the original orbit accurately, it is nevertheless following some nearby true orbit.[14,15] In any case, the average behavior of orbits as a function of equilibrium parameters and initial conditions is clearly seen. As a check of the effects of numerical precision, Fig. 12 includes data points obtained using 128-bit arithmetic (32 digit precision); these results did not differ significantly from those obtained using 64-bit arithmetic.

IV. CONCLUSIONS

We have considered the role of intrinsic chaotic motion on the stability of plasma equilibria with free energy. Free energy permits the existence of negative-energy waves. A system with negative-energy waves, even if linearly stable,

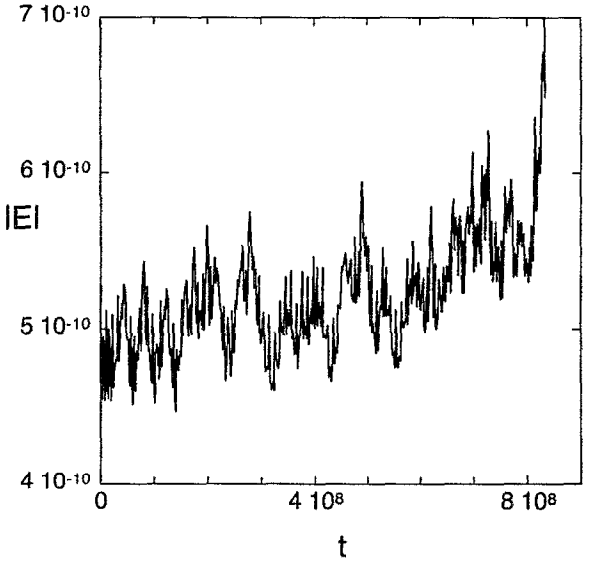

FIG. 10. Electric field magnitude E (in units of $T_e/e\lambda_d$) as a function of time (in ion-acoustic periods) for the points plotted in Fig. 8.

may become nonlinearly unstable due to the resonant interaction of positive- and negative-energy modes. Previous work, which assumed integrable behavior in order to describe the nonlinear explosive instability, was complemented here by consideration of the chaotic motion that is ubiquitous in nonlinear dynamical systems.

Describing a simple example via a Hamiltonian formulation allowed us to exploit the wealth of techniques available for understanding the behavior of such systems. Strict constraints on the phase space structure led to conclusions on what to expect in the nonintegrable case. The same constraints also led us to explore techniques for symplectic integration of the equations of motion. The application of Lie algebraic methods led to a fast explicit numerical algorithm that was used to study a number of simple subsystems of interacting waves. Regions of parameter space near explosive three-wave resonances were examined. Strong two-wave interactions that turned out to be generic for this system led to highly chaotic motion. This was a destabilizing influence, causing fluctuations in wave amplitudes and subsequent explosive growth for initial amplitudes below the critical value calculated for the integrable case of an isolated three-wave resonance, but above the threshold necessary to support the decay instabilities that generate chaotic motion.

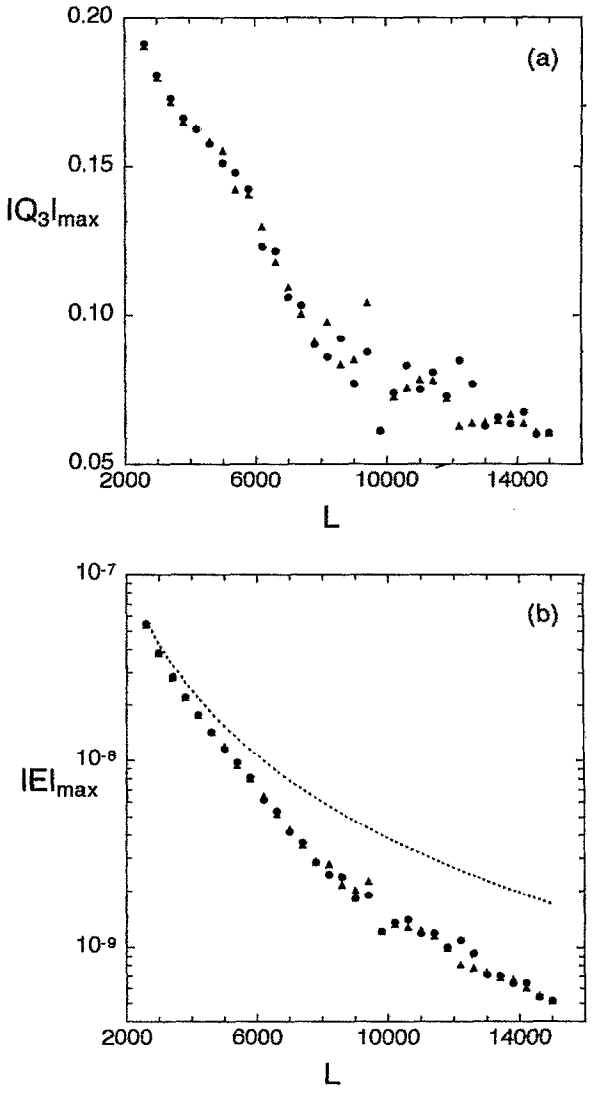

FIG. 12. (a) Largest $|Q_3(0)|$ for which escape had not yet occurred at $t=2\times10^{10}$ ion-acoustic periods, as a function of L; (b) the same data expressed in terms of electric field E, with a dotted line corresponding to $|Q_3(0)|=0.2$. Data indicated by circles are obtained using 64-bit arithmetic; data indicated by triangles are obtained using 128-bit arithmetic.

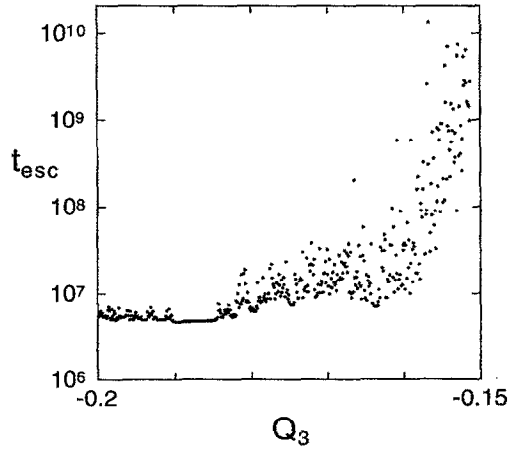

FIG. 11. Escape time in ion-acoustic periods as a function of $Q_3(0)$, for $L=5000$.

This paper considered only a very small portion of the possible parameter space. The glimpses obtained here of the phase space structure and diffusion invite further study, as has been done for other many-dimensional Hamiltonian systems.[16] For more detailed numerical studies of diffusion, it would be desirable to obtain a surface of section mapping describing the time advance between successive intersections with the $\psi_2=\pi/2$ plane in a single iteration. Such mappings have been derived for other Hamiltonians,[17,18] but a satisfactory one has not been obtained for the three degree-of-freedom Hamiltonian of Eq. (22). Such an algorithm

would greatly extend the range of parameters and initial conditions that could be studied, and would facilitate determination of diffusion rates and comparisons to theoretical estimates obtained by Nekhoroshev and others.[19,20] It would also decrease the cumulative numerical error.

While the two and three degree-of-freedom systems considered here represent an improvement over the integrable approximation for three-wave interactions, they still include drastic simplifications. One major approximation is the neglect of a large number of other possible wave–wave interactions, particularly the two-wave interactions that lead to very chaotic motion even when only three waves are involved. At long wavelengths many such interactions can occur simultaneously. The explosive resonances are isolated in parameter space, but the highly chaotic nature of the system broadens the region over which they are important. It would be interesting to carry out further numerical modeling of this system, considering more than three resonances. One would guess that a more realistic number of near-resonant interactions would lead to stronger chaos and faster diffusion than was seen in this paper.

Another effect that might lead to faster diffusion rates is scattering in phase space due to collisions, which is not described by the fluid model developed in this work. The frequency of ion–electron collisions is roughly $\nu/k_1\omega_p \sim \sqrt{m_i/m_e}1/k_1\Lambda^3$.[21] Thus, for $\Lambda=100$ and $L=5000$, the typical time for a collision to occur is $\Delta t\sim 30$ ion-acoustic periods. Collisions might enhance the diffusion rates by scattering orbits off of invariant surfaces and into thin chaotic layers that provide channels for escape.[22] The effect of such extrinsic noise on Hamiltonian systems has been considered by a number of authors.[23–25] This effect might be crudely modeled by incorporating small random perturbations in the numerical algorithm.

Linear Landau damping is not included in the fluid model; this process normally limits the existence of ion-acoustic waves to times shorter than the diffusion time scales considered here.[26] It would be interesting to consider how flattening of the particle distribution functions might eliminate this damping; general nonlinear wave–particle resonance effects such nonlinear Landau damping and particle trapping are of course outside of the fluid model treated.

Other physical systems can also be studied using the methods and concepts described here. The plasma equilibrium considered was chosen partly because it allowed analytical reduction to the simple action-angle form (59) of Part I; this is not possible for all systems. Nevertheless, the $\delta^2 F$ arguments addressing nonlinear stability are widely applicable, and the physical processes considered are quite common, so it is hoped that the results obtained will spur further investigations in these areas.

ACKNOWLEDGMENTS

This work was funded by the U.S. Department of Energy under No. DE-FG05-80ET-53088. One of us (CSK) would like to thank Ivan Gjaja for several helpful conversations on the derivation of explicit algorithms using Lie transforms.

APPENDIX: NUMERICAL ALGORITHM

The Hamiltonian systems studied in this work were visualized graphically using "resonance coordinates." These coordinate systems are convenient for viewing the phase space, but are ill suited for numerical computations. We therefore employ a different set of "computational coordinates," which reduce the Hamiltonians to forms amenable to the Lie transform methods of Sec. II.

Consider first the five degree-of-freedom Hamiltonian (20):

$$H=\omega_1 J_1+\omega_2 J_2+\omega_3 J_3-\omega_4 J_4-\omega_5 J_5 + \alpha J_1\sqrt{J_2}\,\sin(2\theta_1-\theta_2)+\beta J_2\sqrt{J_3}\,\sin(2\theta_2-\theta_3) + \gamma\sqrt{J_2 J_4 J_5}\,\sin(\theta_2+\theta_4+\theta_5). \tag{A1}$$

The transformation to computational variables is obtained from the generating function,

$$F=\hat{I}_1\theta_1+\hat{I}_3\theta_2+\hat{I}_2\theta_3+(\hat{I}_4+\hat{I}_3+2\hat{I}_2+\tfrac{1}{2}\hat{I}_1)\theta_4 + (\hat{I}_4+\hat{I}_3+2\hat{I}_2+\tfrac{1}{2}\hat{I}_1)\theta_5. \tag{A2}$$

This yields the transformation

$$\begin{aligned} &J_1=\hat{I}_1, \quad \hat{\psi}_1=\theta_1+\tfrac{1}{2}(\theta_4+\theta_5),\\ &J_2=\hat{I}_3, \quad \hat{\psi}_2=\theta_3+2(\theta_4+\theta_5),\\ &J_3=\hat{I}_2, \quad \hat{\psi}_3=\theta_2+\theta_4+\theta_5,\\ &J_4=\hat{I}_4+\hat{I}_3+2\hat{I}_2+\tfrac{1}{2}\hat{I}_1, \quad \hat{\psi}_4=\theta_4,\\ &J_5=\hat{I}_5+\hat{I}_3+2\hat{I}_2+\tfrac{1}{2}\hat{I}_1, \quad \hat{\psi}_5=\theta_5, \end{aligned} \tag{A3}$$

giving us the new Hamiltonian

$$\hat{H}=H-\Omega_3\hat{I}_5=\hat{\Omega}_1\hat{I}_1+\hat{\Omega}_2\hat{I}_2+\hat{\Omega}_3\hat{I}_3+\alpha\hat{I}_1\sqrt{\hat{I}_3}\,\sin(2\hat{\psi}_1-\hat{\psi}_3) + \beta\hat{I}_3\sqrt{\hat{I}_2}\,\sin(2\hat{\psi}_3-\hat{\psi}_2) + \gamma\sqrt{\hat{I}_3(\hat{I}_4+\hat{I}_3+2\hat{I}_2+\tfrac{1}{2}\hat{I}_1)(\hat{I}_5+\hat{I}_3+2\hat{I}_2+\tfrac{1}{2}\hat{I}_1)}\sin\hat{\psi}_3, \tag{A4}$$

where the new frequencies,

$$\hat{\Omega}_1=\tfrac{1}{2}(\Omega_1+\Omega_3), \quad \hat{\Omega}_2=\Omega_2+2\Omega_3, \quad \hat{\Omega}_3=\Omega_3, \tag{A5}$$

are expressed in terms of the resonance detunings,

$$\Omega_1=2\omega_1-\omega_2, \quad \Omega_2=\omega_3-2\omega_2, \quad \Omega_3=\omega_2-\omega_4-\omega_5. \tag{A6}$$

For the special case $\hat{I}_4=\hat{I}_5$, we write this in Cartesian coordinates, $\hat{P}_i=\sqrt{2\hat{I}_i}\cos\hat{\psi}_i$ and $\hat{Q}_i=\sqrt{2\hat{I}_i}\sin\hat{\psi}_i$, as follows:

$$\hat{H}=\frac{\hat{\Omega}_1}{2}(\hat{P}_1^2+\hat{Q}_1^2)+\frac{\Omega_2}{2}(\hat{P}_2^2+\hat{Q}_2^2)+\frac{\Omega_3}{2}(\hat{P}_3^2+\hat{Q}_3^2) + \frac{\alpha}{2\sqrt{2}}[2\hat{Q}_1\hat{P}_1\hat{P}_3-\hat{Q}_3(\hat{P}_1^2-\hat{Q}_1^2)] + \frac{\beta}{2\sqrt{2}}[2\hat{Q}_3\hat{P}_3\hat{P}_2-\hat{Q}_2(\hat{P}_3^2-\hat{Q}_3^2)]+\frac{\gamma}{\sqrt{2}}\hat{Q}_3[\hat{I}_{4,5} + \tfrac{1}{4}(\hat{P}_1^2+\hat{Q}_1^2)+(\hat{P}_2^2+\hat{Q}_2^2)+\tfrac{1}{2}(\hat{P}_3^2+\hat{Q}_3^2)]. \tag{A7}$$

We now apply the techniques described in Sec. II to derive a small time step integrator for the Hamiltonian (A7), correct to third order in Δt and to second order in the dynamical variables $\hat{z}_i := (\hat{Q}_i, \hat{P}_i)$. We seek operators of the form

$$z_i' = e^{[f_3,\cdot]} e^{[f_2,\cdot]} z_i . \tag{A8}$$

From the definition of the Lie transform, Eq. (2), the following transformations are easily derived:

$$f = \alpha g(q) \Rightarrow \begin{cases} q' = q, \\ p' = p + \alpha \dfrac{\partial g}{\partial q}, \end{cases} \tag{A9}$$

$$f = \alpha g(p) \Rightarrow \begin{cases} q' = q - \alpha \dfrac{\partial g}{\partial p}, \\ p' = p, \end{cases} \tag{A10}$$

$$f = \alpha p q \Rightarrow \begin{cases} q' = e^{-\alpha} q, \\ p' = e^{\alpha} p, \end{cases} \tag{A11}$$

$$f = \alpha \frac{p^2 - q^2}{2} \Rightarrow \begin{cases} q' = q \cosh \alpha - p \sinh \alpha, \\ p' = -q \sinh \alpha + p \cosh \alpha, \end{cases} \tag{A12}$$

$$f = \alpha \frac{p^2 + q^2}{2} \Rightarrow \begin{cases} q' = q \cos \alpha + p \sin \alpha, \\ p' = -q \sin \alpha + p \cos \alpha. \end{cases} \tag{A13}$$

For cubic polynomials, we use the following formula of Gjaja:[7]

$$f = \alpha p^m q^n,$$

$$m + n = 3 \Rightarrow \begin{cases} q' = q[1 + \alpha(n-m) q^{n-1} p^{m-1}]^{m/(m-n)}, \\ p' = p[1 + \alpha(n-m) q^{n-1} p^{m-1}]^{n/(n-m)}. \end{cases} \tag{A14}$$

We now write the Hamiltonian of Eq. (A7) as

$$H = H_2 + H_3 = H_2 + H_3^{(\alpha)} + H_3^{(\beta)} + H_3^{(\gamma)}, \tag{A15}$$

where H_2 comprises the three terms quadratic in the $\hat{P}_i, \hat{Q}_i$ (linear in the $\hat{I}_i$), and the $H^{(\alpha,\beta,\gamma)}$ are the three terms cubic in the $\hat{P}_i, \hat{Q}_i$ (nonlinear in the $\hat{I}_i$). The function f_2 is given by

$$f_2 = -\hat{H}_2 \, \Delta t, \tag{A16}$$

yielding the linear transformations

$$\begin{bmatrix} \hat{Q}_i' \\ \hat{P}_i' \end{bmatrix} = \begin{bmatrix} \cos(\hat{\Omega}_i \, \Delta t) & \sin(\hat{\Omega}_i \, \Delta t) \\ -\sin(\hat{\Omega}_i \, \Delta t) & \cos(\hat{\Omega}_i \, \Delta t) \end{bmatrix} \begin{bmatrix} \hat{Q}_i \\ \hat{P}_i \end{bmatrix}. \tag{A17}$$

It is easily shown from the Campbell–Baker–Hausdorff formula[3] that our algorithm can be made accurate to order Δt^3 rather than Δt^2 by splitting the linear transformation into two parts:

$$z_i' = e^{[f_2/2,\cdot]} e^{[f_3,\cdot]} e^{[f_2/2,\cdot]} z_i . \tag{A18}$$

This was done in our computations.

The polynomial f_3 is given by

$$f_3 := -\int_0^{\Delta t} dt \; H_3(\hat{z}_i') = f_3^{(\alpha)} + f_3^{(\beta)} + f_3^{(\gamma)}, \tag{A19}$$

where

$$f_3^{(\alpha)} = (A_1 \hat{Q}_3 - A_2 \hat{P}_3)(\hat{Q}_1^2 - \hat{P}_1^2) + 2 \hat{Q}_1 \hat{P}_1 (A_1 \hat{P}_3 + A_2 \hat{Q}_3), \tag{A20}$$

$$f_3^{(\beta)} = (B_1 \hat{Q}_2 + B_2 \hat{P}_2)(\hat{Q}_3^2 - \hat{P}_3^2) + 2 \hat{Q}_3 \hat{P}_3 (B_1 \hat{P}_2 - B_2 \hat{Q}_2), \tag{A21}$$

$$f_3^{(\gamma)} = (C_1 \hat{Q}_3 + C_2 \hat{P}_3)[\tfrac{1}{4}(\hat{P}_1^2 + \hat{Q}_1^2) + (\hat{P}_2^2 + \hat{Q}_2^2) + \tfrac{1}{2}(\hat{P}_3^2 + \hat{Q}_3^2)], \tag{A22}$$

and

$$\begin{aligned} A_1 &= -\frac{\alpha}{\sqrt{8}\Omega_1} \sin(\Omega_1 \, \Delta t), \\ A_2 &= -\frac{\alpha}{\sqrt{8}\Omega_1} 2 \sin^2\left(\frac{\Omega_1 \, \Delta t}{2}\right), \\ B_1 &= -\frac{\beta}{\sqrt{8}\Omega_2} \sin(\Omega_2 \, \Delta t), \\ B_2 &= -\frac{\beta}{\sqrt{8}\Omega_2} 2 \sin^2\left(\frac{\Omega_2 \, \Delta t}{2}\right), \\ C_1 &= -\frac{\gamma}{\sqrt{2}\Omega_3} \sin(\Omega_3 \, \Delta t), \\ C_2 &= -\frac{\gamma}{\sqrt{2}\Omega_3} 2 \sin^2\left(\frac{\Omega_3 \, \Delta t}{2}\right). \end{aligned} \tag{A23}$$

From straightforward application of Eqs. (A9)–(A12), the first two terms of $f_3^{(\alpha)}$ yield the transformations

$$\begin{aligned} \hat{Q}_1' &= \hat{Q}_1 \cosh 2(A_2 \hat{P}_3 - A_1 \hat{Q}_3) - \hat{P}_1 \sinh 2(A_2 \hat{P}_3 - A_1 \hat{Q}_3), \\ \hat{P}_1' &= -\hat{Q}_1 \sinh 2(A_2 \hat{P}_3 - A_1 \hat{Q}_3) + \hat{P}_1 \cosh 2(A_2 \hat{P}_3 - A_1 \hat{Q}_3), \\ \hat{Q}_3' &= \hat{Q}_3 - A_2(\hat{P}_1^2 - \hat{Q}_1^2), \\ \hat{P}_3' &= \hat{P}_3 - A_1(\hat{P}_1^2 - \hat{Q}_1^2) \end{aligned} \tag{A24}$$

and

$$\begin{aligned} \hat{Q}_1' &= \hat{Q}_1 \exp(-2A_1 \hat{P}_3 - 2A_2 \hat{Q}_3), \\ \hat{P}_1' &= \hat{P}_1 \exp(2A_1 \hat{P}_3 + 2A_2 \hat{Q}_3), \\ \hat{Q}_3' &= \hat{Q}_3 - 2A_1 \hat{P}_1 \hat{Q}_1, \\ \hat{P}_3' &= \hat{P}_3 + 2A_2 \hat{P}_1 \hat{Q}_1 . \end{aligned} \tag{A25}$$

The operator $e^{[f_3^{(\beta)},\cdot]}$ has exactly the same form as $e^{[f_3^{(\alpha)},\cdot]}$, and is treated in the same way.

The first two terms inside the bracket of Eq. (A22) yield the transformations,

$$\begin{aligned} \hat{Q}_1' &= \hat{Q}_1 \cos \tfrac{1}{2}(C_1 \hat{Q}_3 + C_2 \hat{P}_3) + \hat{P}_1 \sin \tfrac{1}{2}(C_1 \hat{Q}_3 + C_2 \hat{P}_3), \\ \hat{P}_1' &= -\hat{Q}_1 \sin \tfrac{1}{2}(C_1 \hat{Q}_3 + C_2 \hat{P}_3) + \hat{P}_1 \cos \tfrac{1}{2}(C_1 \hat{Q}_3 + C_2 \hat{P}_3), \\ \hat{Q}_3' &= \hat{Q}_3 - \tfrac{1}{4} C_2(\hat{P}_1^2 + \hat{Q}_1^2), \\ \hat{P}_3' &= \hat{P}_3 + \tfrac{1}{4} C_1(\hat{P}_1^2 + \hat{Q}_1^2) \end{aligned} \tag{A26}$$

and

$$\begin{aligned}
\hat{Q}_2' &= \hat{Q}_2 \cos 2(C_1\hat{Q}_3 + C_2\hat{P}_3) \\
&\quad + \hat{P}_2 \sin 2(C_1\hat{Q}_3 + C_2\hat{P}_3), \\
\hat{P}_2' &= -\hat{Q}_2 \sin 2(C_1\hat{Q}_3 + C_2\hat{P}_3) \\
&\quad + \hat{P}_2 \cos 2(C_1\hat{Q}_3 + C_2\hat{P}_3), \\
\hat{Q}_3' &= \hat{Q}_3 - C_2(\hat{P}_2^2 + \hat{Q}_2^2), \\
\hat{P}_3' &= \hat{P}_3 + C_1(\hat{P}_2^2 + \hat{Q}_2^2).
\end{aligned} \tag{A27}$$

Splitting the remaining term of Eq. (A22) into four monomials yields the four transformations,

$$\begin{aligned}
\hat{Q}_3' &= \hat{Q}_3, \\
\hat{P}_3' &= \hat{P}_3 + \tfrac{3}{2}C_1\hat{Q}_3^2,
\end{aligned} \tag{A28}$$

$$\begin{aligned}
\hat{Q}_3' &= \hat{Q}_3 - \tfrac{3}{2}C_2\hat{P}_3^2, \\
\hat{P}_3' &= \hat{P}_3,
\end{aligned} \tag{A29}$$

$$\begin{aligned}
\hat{Q}_3' &= \hat{Q}_3(1 - C_1\hat{P}_3)^2, \\
\hat{P}_3' &= \hat{P}_3/(1 - C_1\hat{P}_3),
\end{aligned} \tag{A30}$$

$$\begin{aligned}
\hat{Q}_3' &= \hat{Q}_3/(1 + C_2\hat{Q}_3), \\
\hat{P}_3' &= \hat{P}_3(1 + C_2\hat{Q}_3)^2.
\end{aligned} \tag{A31}$$

We now have an explicit symplectic algorithm with which to follow the time evolution of the Hamiltonian (A1). In earlier sections we discussed other Hamiltonians corresponding to subsets of the five modes described by (A1). Computational coordinates for these Hamiltonians could be obtained by simply setting irrelevant coordinates to zero in the generating function (A2). In some cases, however, this would result in Hamiltonians with frequencies $\hat{\Omega}_i$ that are not small compared to the ω_i's. These large frequencies may be eliminated via a preliminary time-dependent canonical transformation to a rotating reference frame. For each of the Hamiltonians considered in this paper, we now indicate the appropriate transformation between the original coordinates (J_i, θ_i) and new coordinates $(\hat{J}_i, \hat{\theta}_i)$. (In each case, we have $\hat{J}_i = J_i$; only the angles are changed.) Once this transformation is carried out, the final transformation from $(\hat{J}_i, \hat{\theta}_i)$ to $(\hat{I}_i, \hat{\psi}_i)$ is obtained from a generating function with the same functional form as Eq. (A2), with θ_i replaced by $\hat{\theta}_i$, and irrelevant terms dropped. Derivation of the algorithms then proceed as above. The time-dependent transformations change only the linear parts of the final algorithms; the nonlinear pieces are unchanged from those derived above, except that modes not included in a given Hamiltonian are set to zero.

The first Hamiltonian considered in Sec. III was (7):

$$H = \omega_1 J_1 + \omega_2 J_2 + \alpha J_1\sqrt{J_2}\,\sin(2\theta_1 - \theta_2). \tag{A32}$$

We employ the time-dependent generating function,

$$F(\hat{\mathbf{J}}, \boldsymbol{\theta}, t) = J_1(\theta_1 - \omega_2 t/2) + \hat{J}_2(\theta_2 - \omega_2 t), \tag{A33}$$

which provides the transformation

$$\begin{aligned}
J_1 &= \frac{\partial F}{\partial \theta_1} = \hat{J}_1, \quad \hat{\theta}_1 = \frac{\partial F}{\partial \hat{J}_1} = \theta_1 - \frac{\omega_2 t}{2}, \\
J_2 &= \frac{\partial F}{\partial \theta_2} = \hat{J}_2, \quad \hat{\theta}_2 = \frac{\partial F}{\partial \hat{J}_2} = \theta_2 - \omega_2 t.
\end{aligned} \tag{A34}$$

The new Hamiltonian is given by

$$\begin{aligned}
\hat{H}(\hat{\mathbf{J}}, \hat{\theta}) &= H[\mathbf{J}(\hat{\mathbf{J}}), \boldsymbol{\theta}(\hat{\theta}, t)] + \frac{\partial F[\mathbf{J}, \boldsymbol{\theta}(\hat{\theta}, t)]}{\partial t} \\
&= \frac{\Omega_1}{2}\hat{J}_1 + \alpha\hat{J}_1\sqrt{\hat{J}_2}\,\sin(2\hat{\theta}_1 - \hat{\theta}_2).
\end{aligned} \tag{A35}$$

Now, using a generating function analogous to (A2), we obtain the final transformation to computational coordinates:

$$\begin{aligned}
\hat{J}_1 &= \hat{I}_1, \quad \hat{\psi}_1 = \hat{\theta}_1, \\
\hat{J}_2 &= \hat{I}_3, \quad \hat{\psi}_2 = \hat{\theta}_3,
\end{aligned} \tag{A36}$$

giving us the new Hamiltonian

$$\hat{H} = \frac{\Omega_1}{2}\hat{I}_1 + \alpha\hat{I}_1\sqrt{\hat{I}_3}\,\sin(2\hat{\psi}_1 - \hat{\psi}_3). \tag{A37}$$

The other integrable Hamiltonian that was studied numerically was (10); in this case straightforward application of (A2) yields a Hamiltonian whose frequency is equal to the detuning Ω_3, so that no preliminary coordinate transformation is necessary.

Now consider the Hamiltonian (17):

$$\begin{aligned}
H &= \omega_1 J_1 + \omega_2 J_2 + \omega_3 J_3 + \alpha J_1\sqrt{J_2}\,\sin(2\theta_1 - \theta_2) \\
&\quad + \beta J_2\sqrt{J_3}\,\sin(2\theta_2 - \theta_3).
\end{aligned} \tag{A38}$$

We employ a transformation obtained from the generating function

$$\begin{aligned}
F(\hat{\mathbf{J}}, \boldsymbol{\theta}, t) &= \hat{J}_1[\theta_1 - (4\omega_2 - \omega_3)t/4] + \hat{J}_2[\theta_2 - (4\omega_2 \\
&\quad - \omega_3)t/2] + \hat{J}_3[\theta_3 - (4\omega_2 - \omega_3)t],
\end{aligned} \tag{A39}$$

to obtain the new Hamiltonian,

$$\begin{aligned}
\hat{H}(\hat{\mathbf{J}}, \hat{\theta}) &= (\tfrac{1}{2}\Omega_1 + \tfrac{1}{4}\Omega_2)\hat{J}_1 + 2\Omega_2\hat{J}_2 + \tfrac{1}{2}\Omega_2\hat{J}_3 \\
&\quad + \alpha\hat{J}_1\sqrt{\hat{J}_2}\,\sin(2\hat{\theta}_1 - \hat{\theta}_2) \\
&\quad + \beta\hat{J}_2\sqrt{\hat{J}_3}\,\sin(2\hat{\theta}_2 - \hat{\theta}_3).
\end{aligned} \tag{A40}$$

The final transformation is

$$\begin{aligned}
\hat{J}_1 &= \hat{I}_1, \quad \hat{\psi}_1 = \hat{\theta}_1, \\
\hat{J}_2 &= \hat{I}_3, \quad \hat{\psi}_2 = \hat{\theta}_3, \\
\hat{J}_3 &= \hat{I}_2, \quad \hat{\psi}_3 = \hat{\theta}_2.
\end{aligned} \tag{A41}$$

[1] C. S. Kueny and P. J. Morrison, Phys. Plasmas **2**, 1926 (1995).
[2] G. Haller and S. Wiggins, "Geometry and chaos near resonant equilibria of 3-DOF Hamiltonian systems I: Theory," to appear in Physica D.
[3] A. J. Dragt and J. Finn, J. Math. Phys. **17**, 2215 (1976).
[4] A. J. Dragt and E. Forest, J. Math. Phys. **24**, 2734 (1983).
[5] J. Irwin, in *Accelerator Physics at the Superconducting Super Collider*, edited by Y. T. Yan, J. P. Naples, and M. J. Syphers (American Institute of Physics, New York, 1995), pp. 662–669.

[6]G. Rangarajan, A. J. Dragt, and F. Neri, Part. Accel. **28**, 119 (1990).
[7]I. Gjaja, Part. Accel. **43**, 133 (1994).
[8]P. J. Channel and C. Scovel, Nonlinearity **3**, 231 (1990).
[9]J. R. Cary, Bull. Am. Phys. Soc. **34**, 1927 (1989).
[10]J. M. Sanz-Serna, Physica D **60**, 293 (1992).
[11]C. S. Kueny, "Nonlinear instability and chaos in plasma wave–wave interactions," Ph.D. thesis, University of Texas at Austin, 1993.
[12]B. V. Chirikov, Phys. Rep. **52**, 265 (1979).
[13]M. A. Lieberman and J. L. Tennyson, in *Long-Time Prediction in Dynamics*, edited by C. W. Horton, Jr., L. E. Reichl, and V. G. Szebehely (Wiley, New York, 1983), pp. 179–211.
[14]S. Hammel, J. A. Yorke, and C. Grebogi, Complexity **3**, 136 (1987).
[15]S. Hammel, J. A. Yorke, and C. Grebogi, Bull. Am. Math. Soc. **19**, 465 (1988).
[16]H. Kook, "Chaotic transport in Hamiltonian dynamical systems with several degrees of freedom," Ph.D. thesis, University of Texas at Austin, 1989.
[17]A. J. Lichtenberg and M. A. Lieberman, *Regular and Stochastic Motion* (Springer-Verlag, New York, 1983), p. 157.
[18]C. S. Kueny and P. J. Morrison, Bull. Am. Phys. Soc. **33**, 1875 (1988).
[19]N. N. Nekhoroshev, Russ. Math. Surveys **32**, 1 (1977).
[20]G. Benettin and G. Gallavotti, J. Stat. Phys. **44**, 293 (1986).
[21]D. R. Nicholson, *Introduction to Plasma Theory* (Wiley, New York, 1983), p. 14.
[22]B. V. Chirikov, Sov. J. Plasma Phys. **4**, 289 (1978).
[23]B. V. Chirikov, Sov. J. Plasma Phys. **5**, 492 (1979).
[24]R. H. Cohen and G. Rowlands, Phys. Fluids **24**, 2295 (1981).
[25]J. L. Tennyson, Physica D **5**, 123 (1982).
[26]N. A. Krall and A. W. Trivelpiece, *Principles of Plasma Physics* (McGraw-Hill, New York, 1973), p. 391.